http://dx.doi.org/10.5012/bkcs.2012.33.5.1653

# Highly Crystalline 2,6,9,10-Tetrakis((4-hexylphenyl)ethynyl)anthracene for Efficient Solution-Processed Field-effect Transistors

**Jung A Hur, Jicheol Shin, Tae Wan Lee, Kyung Hwan Kim, Min Ju Cho, and Dong Hoon Choi***

*Department of Chemistry, Research Institute for Natural Sciences, Korea University, Seoul 136-701, Korea*
**E-mail: dhchoi8803@korea.ac.kr*
*Received December 19, 2011, Accepted February 16, 2012*

A new anthracene-containing conjugated molecule was synthesized through the Sonogashira coupling and reduction reactions. 1-Ethynyl-4-hexylbenzene was coupled to 2,6-bis((4-hexylphenyl) ethynyl)anthracene-9,10-dione through a reduction reaction to generate 2,6,9,10-tetrakis((4-hexylphenyl)ethynyl) anthracene. The semiconducting properties were evaluated in an organic thin film transistor (OTFT) and a single-crystal field-effect transistor (SC-FET). The OTFT showed a mobility of around 0.13 $cm^2 V^{-1} s^{-1}$ ($I_{ON}/I_{OFF} > 10^6$), whereas the SC-FET showed a mobility of 1.00-1.35 $cm^2 V^{-1} s^{-1}$, which is much higher than that of the OTFT. Owing to the high photoluminescence quantum yield of 2,6,9,10-tetrakis((4-hexylphenyl)ethynyl) anthracene, we could observe a significant increase in drain current under irradiation with visible light ($\lambda$ = 538 nm, 12.5 $\mu W/cm^2$).

**Key Words :** Organic semiconductor, Conjugated molecule, Thin film transistor, Field-effect transistor, Photoresponsivity

## Introduction

Research has focused on replacing vacuum-processable materials with solution-processable materials to overcome severe limitations in large-scale device fabrication due to the complexity of the process.[1,2] Soluble p-type organic semiconductors have become important materials for the fabrication of high-performance organic thin film transistors (OTFTs) with high hole mobilities of the order of 1 $cm^2 V^{-1} s^{-1}$.[3-5]

Among various kinds of soluble organic semiconductors, two-dimensional π-extended conjugated molecular structures in the form of films have shown effective charge-transport properties, satisfying the requirements for soluble semiconducting materials.[6,7] It is well recognized that the electronic structure, molecular structure, and morphology of thin films are important for enhancing carrier mobility in OTFT devices. Among these three requirements, thin film morphology has been recognized as being the most important requirement for enhancing the charge-transport phenomenon. Crystallization induced by J-aggregation in the solid state improves the slip-stacked charge-transport phenomenon, thus enhancing the carrier mobility in OTFTs. In addition, a single-crystal-based field effect transistor (FET) can exhibit fully optimized semiconducting properties.

In order to improve the crystallinity in the solid state, the conjugated molecules should have a planar structure and strong intermolecular interaction. As a trade-off problem, highly crystalline conjugated molecules satisfying above requirements, the molecules show very poor solubility in organic solvent; therefore, solution processing to fabricate the devices is hard to be achieved successfully. The role of aliphatic peripheral-groups is two-fold: (1) to increase the solubility of the compounds, and (2) to induce lateral molecule-to-molecule recognition within a single molecular layer.[8-10] Two X-shaped our previous molecules whose structures are quite similar to the molecules in this study, they contain only two alkyl peripheral moieties in one molecule.[11] Compared to those molecules, 2,6,9,10-tetrakis((4-hexylphenyl)ethynyl) anthracene used in this study showed much improved solubility, which facilitate the solution processing less costly. We find that additional side aliphatic group enhances not only the solubility but also the degree of self-organization.

In this work, we present an intriguing π-conjugated molecule, 2,6,9,10-tetrakis((4-hexylphenyl)ethynyl) anthracene. Our molecular design involves the introduction of four hexyl peripheral groups for improving the solubility and degree of crystallinity in the film states. It provides the strong molecular self-association to form a single-crystalline microplates too. The proposed molecules exhibited quite promising carrier mobility both in thin film transistor (TFT) and single-crystalline plate field-effect transistors (FET). In addition due to its high photoluminescence quantum yield, the performance as a phototransistor could be investigated.

## Experimentals

### Synthesis.

**Materials:** All commercially available starting materials and solvents were purchased from Aldrich, TCI, and Acros Co. and used without further purification. All of the reactions and manipulations were carried out under $N_2$ with the use of standard inert-atmosphere and Schlenk techniques unless otherwise noted. Solvent used in inert-atmosphere reactions were dried and degassed using standard proce-

dures. Column chromatography was carried out with 230-400 mesh silica gel from Aldrich using wet-packing method. All deuterated solvent were purchased from Cambridge Isotope Laboratories, Inc.

**2,6-Bis((4-hexylphenyl)ethynyl)anthracene-9,10-dione, 2:** 2,6-Dibromoanthracene-9,10-dione (3.00 g, 8.2 mmol) was dissolved in in a mixture of freshly distilled THF (80 mL), triethylamine (35 mL) and diisopropylamine (25 mL) in the presence of bis(triphenylphosphine)palladium(II) dichloride (0.29 g, 0.41mmol), and copper iodide (0.078 g, 0.41 mmol). 1-Ethynyl-4-hexylbenzene (3.35 g, 18.0mmol) was then added and the mixture was heated at 80 °C for 16 hrs. After completing the reaction, the solution was poured into methanol to collect the precipitates. The crude solid was purified by silica-gel column chromatography using chloroform as an eluent. Further purification by precipitation afforded **2** (Yield 3.6 g, 74%); $^1$H NMR (400 MHz, $CDCl_3$) δ 8.36 (s, 2H), 8.26-8.24 (d, $J$ = 7.8 Hz, 2H), 7.85-7.83 (d, $J$ = 8.0 Hz, 2H), 7.47-7.45 (d, $J$ = 8.2 Hz, 4H), 7.18-7.16 (d, $J$ = 7.8 Hz, 4H), 2.61-2.65(t, $J$ = 7.8 Hz, 4H), 1.57-1.64 (m, 4H), 1.29-1.34 (m, 12H), 0.87-0.91 (t, $J$ = 6.2 Hz, 6H). $^{13}$C NMR (100 MHz, $CDCl_3$) δ 182.18, 144.77, 136.58, 133.68, 132.20, 132.05, 130.33, 130.26, 128.84, 127.61, 119.56, 95.17, 87.80, 36.20, 31.89, 31.36, 29.15, 22.81, 14.30. LR-MS (EI) *m/z* ($M^+$): Calcd for $C_{42}H_{40}O_2$, 576.3; found, 576.3. EA analysis calcd for $C_{42}H_{40}O_2$: C, 87.46; H, 6.99, found: C, 87.30; H, 6.89.

**2,6,9,10-Tetrakis((4-hexylphenyl)ethynyl)anthracene, 3:** In a 250 mL, oven dried, mag.-stirred RBF, **2** (0.79 g, 4.23 mmol) was dissolved in freshly distilled THF (50 mL). The solution was then cooled to −78 °C. *n*-BuLi (2.03 mL, 5.07 mmol, 2.5 M sol'n. in hexane) was then added dropwise over 15 minutes. This mixture was stirred for 30 min and 2,6-bis((4-hexylphenyl)ethynyl)anthracene-9,10-dione, **1** (1.0 g, 1.69 mmol) were added at −78 °C. The mixture was stirred at room temperature for 3 hrs, and then quenched with water, $SnCl_2$, and HCl. After completing the reaction, the solution was poured into methanol to collect the precipitates. The crude solid was purified by recrystallization from acetone to give 2,6,9,10-tetrakis((4-hexylphenyl)-ethynyl)anthracene (Yield 1.06 g, 68%).

$^1$H-NMR (400 MHz, $CDCl_3$) δ 8.79 (s, 2H), 8.60 (d, $J$ = 8.2 Hz, 2H), 7.72 (d, $J$ = 8.2 Hz, 4H), 7.68 (d, $J$ = 9.0 Hz, 2H), 7.56 (d, $J$ = 8.2 Hz, 4H), 7.29 (d, $J$ = 8.6 Hz, 4H), 7.21 (d, $J$ = 8.2 Hz, 4H), 2.70-2.62 (m, 8H), 1.68-1.61 (m, 8H), 1.34 (m, 24H), 0.92 (t, $J$ = 6.6 Hz, 12H). $^{13}$C NMR (100 MHz, $CDCl_3$) δ 144.17, 143.73, 131.81, 131.71, 131.47, 130.59, 129.34, 128.70, 128.51, 127.44, 121.93, 120.30, 120.23, 118.25, 103.22, 91.73, 89.54, 85.36, 36.04, 31.72, 31.29, 31.23, 22.60, 14.10. HR-MS (FAB) *m/z* ($M^+$): Calcd for $C_{70}H_{74}$, 914.5791; found, 914.5794. EA analysis calcd for $C_{70}H_{74}$: C, 91.85; H, 8.15, found: C, 91.84 ; H, 8.13.

**Instrumentation.** $^1$H NMR spectra were recorded on a Varian Mercury NMR 400 Hz spectrometer using deuterated chloroform purchased from Cambridge Isotope Laboratories, Inc. Elemental analyses were performed using an EA1112 (Thermo Electron Corp.) elemental analyzer. High resolution mass analysis was performed on a JMS-700 M Station mass spectrometer (JEOL, resolution 60,000, *m/z* range at full sensitivity 2,400). Thermal properties were studied under a nitrogen atmosphere on a Mettler DSC 821$^e$ instrument. Thermal gravimetric analysis (TGA) was conducted on a Mettler TGA50 (temperature rate 10 °C/min under $N_2$). Powder X-ray diffraction measurements were recorded with a Rigaku D/MAX Ultima III using nickel-filtered Cu Kα radiation (λ = 1.5418 Å) over a range of 2° < 2θ < 40° and X'celerator detector operating at 40 kV and 30 mA.

The redox properties of two molecules were examined by using cyclic voltammetry (Model: EA161 eDAQ). Thin films were coated on a platinum plate using chloroform as a solvent. The electrolyte solution employed was 0.10 M tetrabutylammoniumhexafluorophosphate ($Bu_4NPF_6$) in a freshly dried acetonitrile. The Ag/AgCl and Pt wire (0.5 mm in diameter) electrodes were utilized as reference and counter electrodes, respectively. The scan rate was at 50 mV/s.

In order to study absorption behavior, the films of two molecules were fabricated on quartz substrates as follows. The solution (1 wt %) of each molecule in chloroform was filtered through an acrodisc syringe filter (Millipore 0.45 μm) and subsequently spin-cast on the quartz glass. The films were dried overnight at 60 °C for 12 hr under vacuum. Absorption spectra of samples in a film and solution state (chloroform, conc. $1 \times 10^{-5}$ mole/L) were obtained using a UV-Vis spectrometer (HP 8453, photodiode array type) in the wavelength range of 190-1100 nm. PL spectra of the solutions were acquired on a Hitachi F-7000 fluorescence spectrophotometer.

**Fabrication of Organic Field-Effect Transistor.** For the characterization of TFT performance, bottom gate top contact device geometry was employed. On the heavily *n*-doped $Si/SiO_2$ substrate the spin-coated films (thickness ~40-50 nm) were prepared with chloroform as a solvent. Surface modification was carried out with *n*-octyltrichlorosilane (OTS) to make hydrophobic dielectric surface. Source and drain electrodes were then thermally evaporated (100 nm) through shadow mask with the channel width and length of 1500 μm and 100 mm, respectively. Particularly, crystalline microplates were grown directly on an OTS-treated $SiO_2/Si$ substrate *via* slow solvent diffusion. (solvents: THF and MeOH) All the field effect mobilities were extracted in the saturation regime using the relationship $\mu_{sat}=(2I_{DS}L)/(WC(V_G-V_{th})^2)$, where $I_{DS}$ means saturation drain current, $C$ is capacitance of $SiO_2$ dielectric (thickness = 300 nm), $V_G$ is gate bias, and $V_{th}$ is threshold voltage. The device performance was evaluated in air using Keithley 4200-SCS semiconductor characterization systemat ambient conditions.

For the light source, a Xenon lamp (Thermo Oriel) equipped with an optical fiber and high-speed monochromator (Oriel Cornerstone$^{TM}$ 130 1/8 m Monochromator) were employed. The light illumination power was measured by a Newport 2385-C Si photodetector with a calibration module. To obtain the PL absolute quantum yields (PLQY) of **3**, absolute PL quantum yield measurement system, C9920-02 DynaSpect Series, (Hamamatsu Photonics, Japan) was em-

ployed.

## Results and Discussion

For this study, we successfully synthesized the a new conjugated molecule, **3** through reduction and Sonogashira coupling reaction. 2,6-Dibromoanthracene-9,10-dione was synthesized according to an established method.[12,13] The addition of the dione compound to two molar equivalents of 1-ethynyl-4-hexylbenzene in the presence of bis(triphenylphosphine) palladium(II) dichloride and copper iodide afforded **1**. The reduction reaction using tin chloride in an acidic medium gave the desired compound, **3**. We show that the hexyl side group enhances not only the solubility but also the degree of self-organization.

It should be noted that 2,6,9,10-tetrakis(phenylethynyl)-anthracene is not soluble in common organic solvents. After tethering hexyl chains to four phenyl rings, the molecule showed good solubility (> 15 mg/1 mL of chloroform for **3**). Scheme 1 illustrates the simple synthetic route for **3**. The identity and purity of **3** were confirmed by $^{1}$H NMR, $^{13}$C NMR, HRMS, and elemental analysis.

The thermal properties of the molecule **3** were characterized by differential scanning calorimetry (DSC) and thermogravimetric analysis (TGA) (see Figure 1). DSC measurements were performed under nitrogen with the highest temperature limited to below the decomposition temperature. Although very small endothermic peak at around 165 °C, molecule **3** exhibited distinct crystalline-isotropic transition temperatures of 180 °C and cold crystallization temperatures of 117 °C. TGA measurements revealed that the molecule **3** had good thermal stability ($T_d$ = 426 °C).

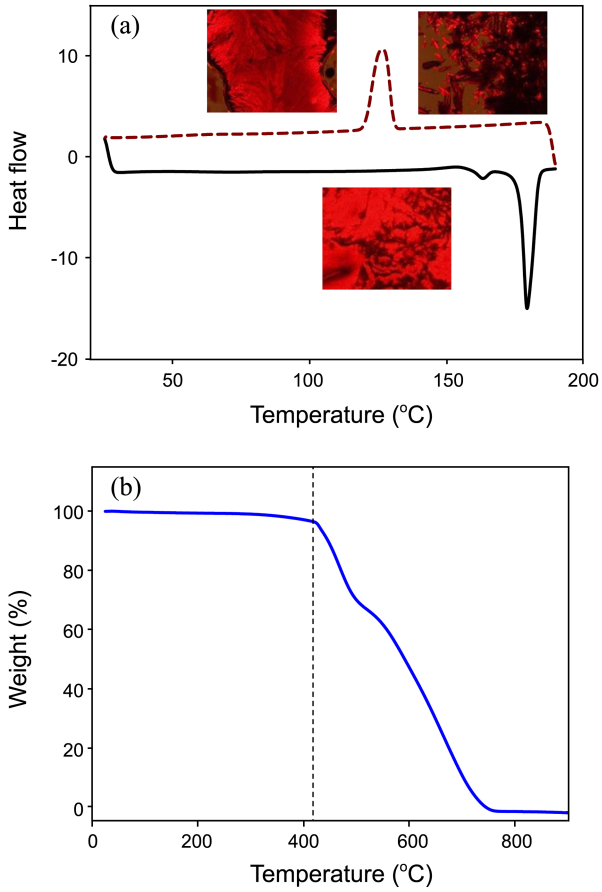


**Figure 1.** Thermal analysis of anthracene-cored semiconducting molecule, **3**. (a) DSC thermogram. Inset: optical microscopic images of crystalline phase. (b) TGA thermogram.

To study the intermolecular interactions between the molecules, absorption spectra of the samples in chloroform (conc. 1 × $10^{-6}$ mole/L) and of the thin films (*i.e.*, as-spun and thermally annealed films) were obtained (Figure 2(a)). We observed a significant bathochromic shift ($\Delta\lambda$ ~ 57-60 nm) and well-resolved vibronic transition bands in the absorption spectra upon film formation, indicating the generation of strong intermolecular interactions. In contrast to the solution phase spectra, the spectra of the spin-cast films were more structured. Figure 2(b) shows the emission spectra of **3** under an excitation wavelength of 371 nm. The emission spectrum of the thermally annealed film exhibited

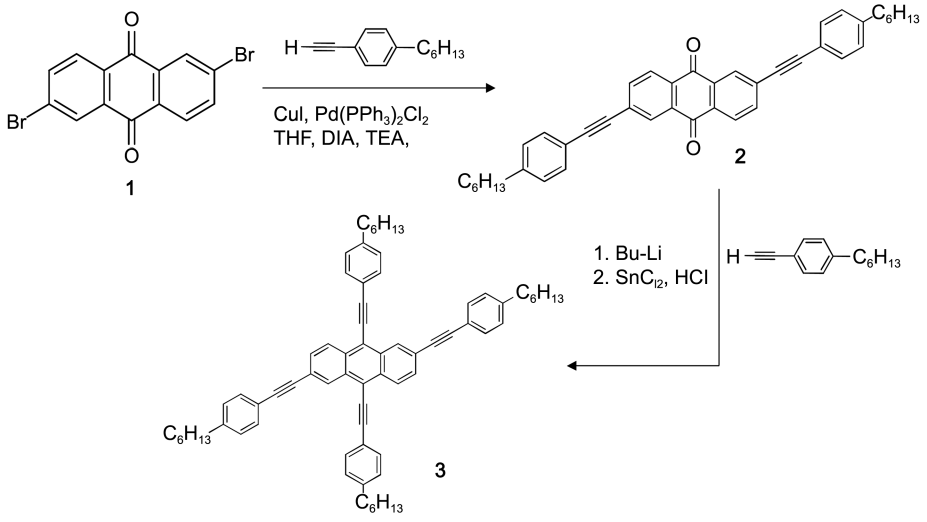


**Scheme 1.** Synthetic procedure for anthracene-cored semiconducting molecule, **3**.

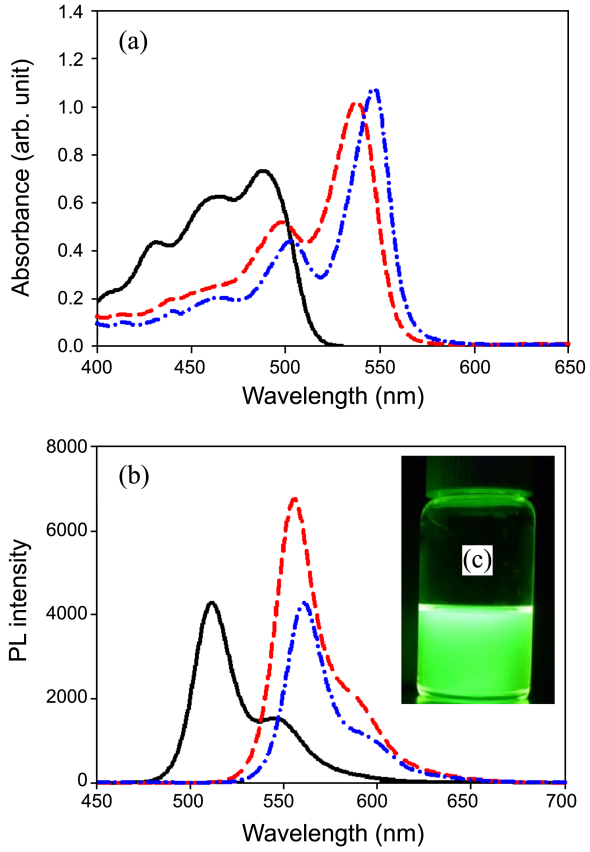


**Figure 2.** UV-Vis absorption spectra (a) and photoluminescence spectra (b) of anthracene-cored semiconducting molecule, **3**. (c) Fluorescence image of the solution. *Absolute quantum yield; solution (97.1% under λ = 488 nm), film (20.4 % under λ = 538 nm); solution (solid line), as-spun film (dashed line), and thermally annealed film (dash-dot-dash line).

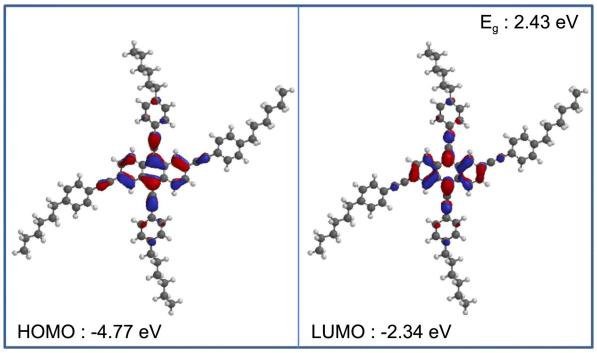


**Figure 3.** HOMO/LUMO levels of molecule **3** used to calculate the theoretical molecular orbitals.

very small red-shift accompanying with the shift of the absorption spectrum. It indicates that no significant annealing effect could be observed on the absorption and emission spectra of **3**. For instance, a non-aggregated emission band appeared at 553 nm and the emission band at 588 nm can be assigned to the J-aggregated characteristic band. It was well consistent with the result in our previous literature.[14]

To estimate the position and molecular energies of frontier orbitals for **3**, Density Functional Theory (DFT) calculations

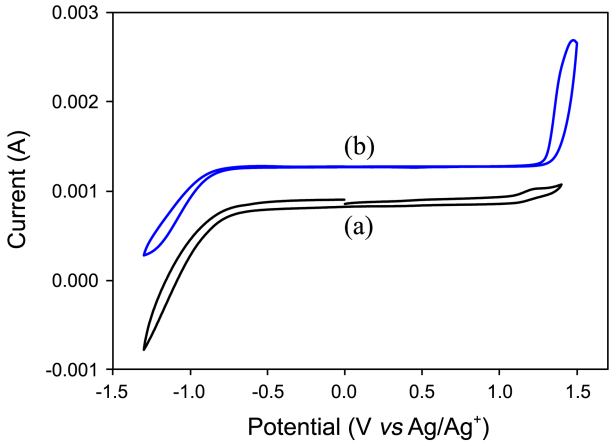


**Figure 4.** Cyclic voltammograms ofanthracene-cored semiconducting molecule, **3**. (a) solution, (b) film. The onset voltage in an oxidation wave was selected to be the oxdiation potential of each molecule.

were performed using the Spartan'06 program at the B3LYP/6-31G* level. The hexyl peripheral groups were sustained in calculation to observe the effect of substituents on the optimized geometries and theoretical energy levels. As shown in Figure 3, the largest coefficients in the HOMO orbitals are located on the 2-D π-system centered at anthracene unit. The coefficients in the LUMO orbital are mainly located on the anthracene unit along 9,10-substituted positions only. It shows that the planarity of conjugated unit was sustained with a small degree of disorder around the hexyl substituents. Under the theroretical calculation, we performed the electrocehmical analysis to determined highest occupied molecular orbital (HOMO) and lowest unoccupied molecular orbital (LUMO) energies of molecule **3**.

To elucidate the HOMO and LUMO energy levels of **3**, the electrochemical properties were investigated by cyclic voltammetry. Cyclic voltammograms (CV) were recorded on solution and film samples, and the potentials were obtained relative to an internal ferrocene reference ($Fc/Fc^+$). These CV scans in the range of −1.5 V to +1.7 V (*vs* Ag/AgCl) show quasi-reversible oxidation peaks. Unfortunately, the reduction behaviors were irreversible; therefore, we were unable to accurately estimate their HOMO and LUMO energies.

To determine the LUMO levels, we combined the oxidation potential in CV with the optical energy bandgap ($E_g^{opt}$) resulting from the absorption edge in the absorption spectrum. Voltammogram of **3** in film form show that the lowest oxidative waves are at around 1.30 V, commonly ($E_{ox}^{onset}$ = +1.04 V for **3** solution). The films have HOMO level of −5.70 eV for **3**. In addition, **3** has LUMO energy levels of around −3.48 eV.

Using slow diffusion of tetrahydrofuran (THF) solutions over MeOH, we obtained microscopic crystalline objects. Analysis by scanning electron microscopy (SEM) revealed that these crystalline objects were collections of hexagonal or rhombus plates of **3** with sizes ranging from several micrometers to tens of micrometers (see Figure 5(a)).

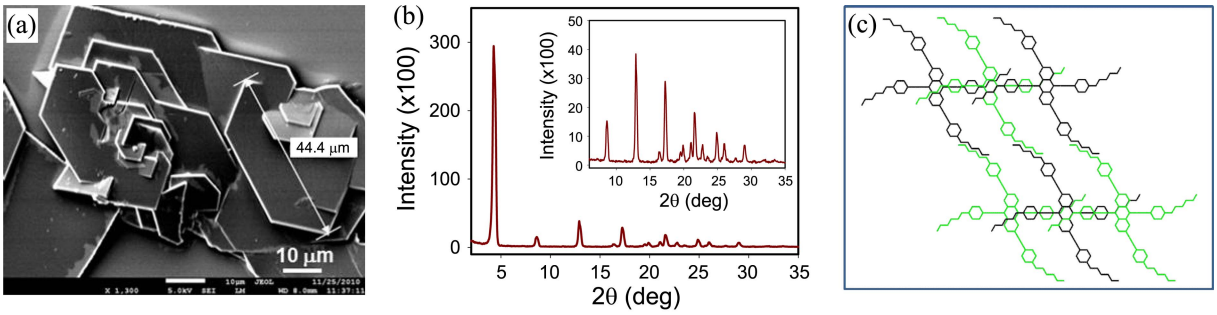


**Figure 5.** (a) SEM image of single-crystalline plates. (b) XRD spectrum of thin film made of **3**. (c) Schematic diagram of molecular packing geometry.

The thin film casted by spin coating method was employed to the X-ray diffraction (XRD) spectrum shown in Figure 5(b). Clear lamella spacings were defined due to the appearance of the peaks at 4.25° (d = 20.80 Å), 8.60° (d = 10.29 Å), and 17.25° (d = 5.14 Å). Therefore, we could expect the formation of well-defined polycrystalline thin films when fabricating thin film transistor as an active layer. Expected molecular packing diagram was proposed in Figure 5(c). Resulting from the absorption spectral data showing the possible J-aggregation between the molecules, they are subject to be aligned along the 9,10-position in an anthracene ring and the underneath molecules were aligned in a J-type stacking manner. The proposed molecular packing geometry can help the slip-stacked charge transort phenomenon between the molecules in TFT and other FET devices.

To examine the potential applications in OTFTs, we investigated the charge-transport properties of **3**. A 400-nm thin film of the semiconductor was deposited by spin-coating a 1 wt % solution of the molecules in chloroform without thermal annealing. The channel length (L) was 100 μm, and the channel width (W) was 1500 μm. Crystalline microplates were grown directly on an OTS-treated $SiO_2$/Si substrate *via* slow solvent diffusion, and bottom-gate top-contact FET devices were fabricated using gold as both the source and drain electrodes. The electrical characterization of TFT and SC-FET devices were illustrated in Figure 6. Figures (a) and (b) showed the device performances of the

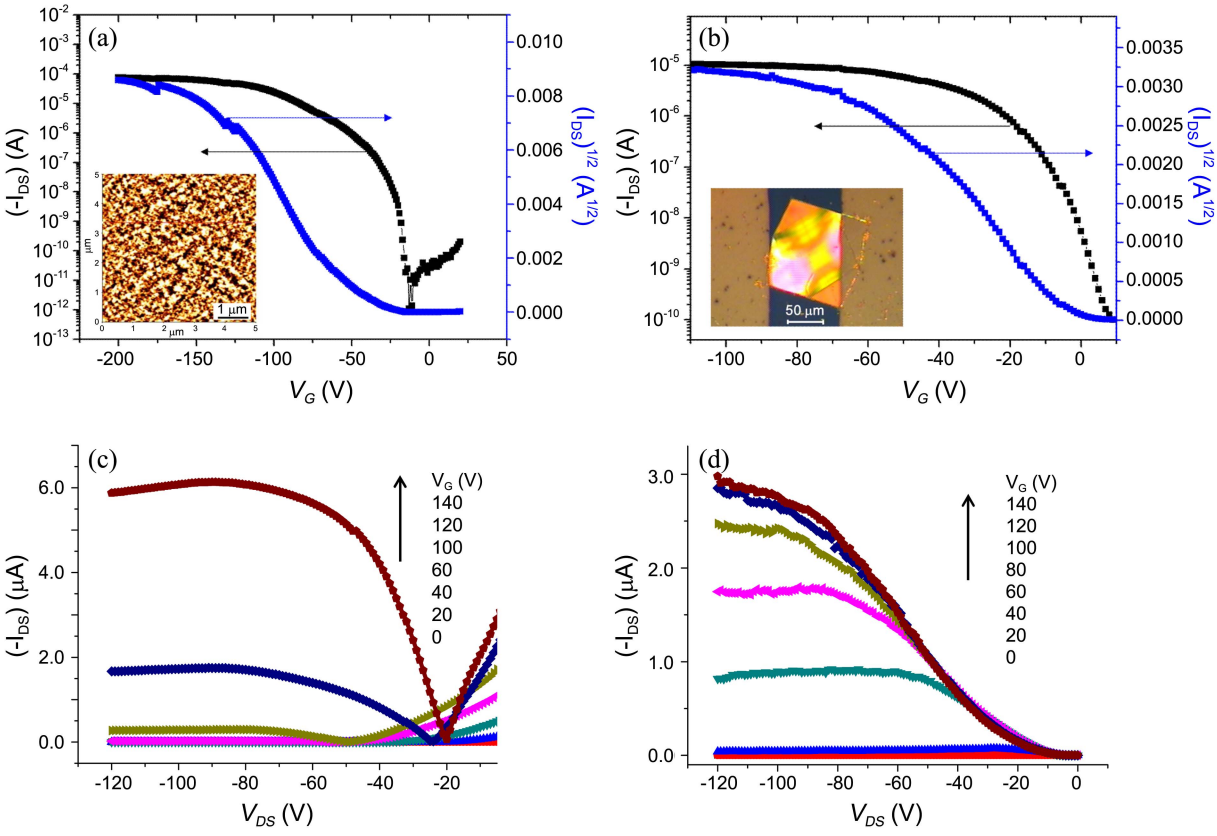


**Figure 6.** (a) Transfer characteristics of the OTFT device. ($V_{DS}$ = −120 V) *Inset: AFM image of the surface of OSC layer. (b) Output curves of the OTFT device. (c) Transfer characteristics of SC-FET device. ($V_{DS}$ = −120 V) *Inset: optical microscopic image of SC-FET device. (d) Output curves of the SC-FET device.

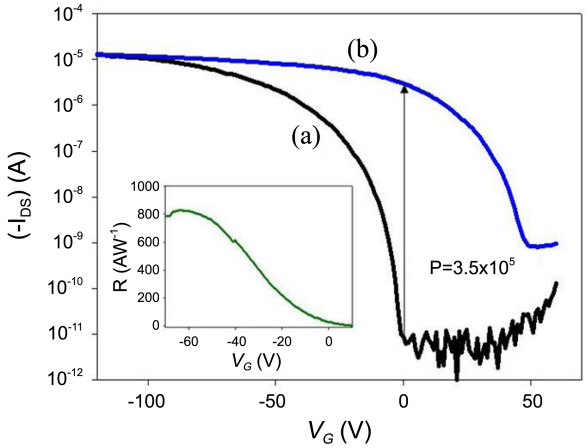


**Figure 7.** Transfer characteristics of organic phototransistor (a) in the dark and (b) under light irradiation with 12.9 μWcm$^{-2}$, λ = 538 nm. *Inset: *R vs.* $V_G$ for the crystalline microplate FET.

TFT device. Figures (c) and (d) showed the device performances of the SC-FET device. The inset in Figure 6(a) shows an atomic force microscopic (AFM) image of the surface of the OSC layer. The inset in Figure 6(c) shows an optical microscopic (OM) image of a crystalline microplate FET. Mobility values were obtained by measuring more than 10 different devices. According to transfer characteristics, the crystalline microplate FETs provided field-effect mobilities of approximately 1.00-1.35 cm$^2$ V$^{-1}$ s$^{-1}$ ($V_{DS}$ = –120 V, channel width: 47.0-63.5 μm) which is approximately 7-10 times higher than the maximum mobility of the OTFT device (μ = 0.13 cm$^2$ V$^{-1}$ s$^{-1}$, $V_{DS}$ = –120 V from Figure 6(a)).

FETs made of crystalline microplates from **3** displayed photoinduced enhancement of the source-drain current ($I_{DS}$). (see Figure 7) Anewphototransistor (PT) devicewas successfully operated because of its high absolute PL quantum yields (PLQYs) in solution state (Φ = 0.97, λ = 488 nm) and film state (Φ = 0.20, λ = 538 nm). It should be noted that the significant increase in $I_{DS}$ was induced by the illumination of low-intensity light ($I_{photo}/I_{dark} > 3 \times 10^5$ at 12.9 μW cm$^{-2}$, λ = 538 nm). The large increase in drain current and the large photoresponsivity ($R$) in an OPT are due to the fact that photogenerated electrons are trapped in the organic layer. These trapped negative charges lead to the injection and accumulation of additional holes in the active layer, thereby increasing the drain current although the gate voltage was removed.[14,15] The accumulated charges can act as an application of gate electric field. We calculated the $R$, defined as $\Delta I_{DS}/P_{inc}$, where $\Delta I_{DS}$ is $I_{DS}^{light} - I_{DS}^{dark}$ and $P_{inc}$ is the incident light intensity. The photoswitching ratio, $(I_{DS}^{light} - I_{DS}^{dark})/I_{DS}^{dark}$, was denoted by $P$. In the inset in Figure 7, $R$ is plotted *versus* $V_G$. The crystalline microplate phototransistor (PT) device showed a relatively high $P$ ($> 3 \times 10^5$, $V_G$ = –1.0 V). The maximum $R$ of the single-crystalline microplate-based PTs was in the range of 250-400 AW$^{-1}$. The measured $R$ is comparable or slightly higher than that of inorganic single-crystal silicon FETs (> 300 AW$^{-1}$, λ = 550 nm, I = 400 μW cm$^{-2}$).[16]

## Conclusion

In conclusion, we successfully synthesized and characterized new anthracene-based conjugated molecule that is solution processable. Molecule **3**, bearing 1-ethynyl-4-hexylbenzenesubsitituents at 2,6- and 9,10-positions in the anthracene ring, showed good solubility in common organic solvent and showed very high crystallinity. Remarkably, the device bearing the crystalline microplate of **3** showed very high carrier mobility, indicating that the uniform lamella and π-stacking of molecule **3** facilitate carrier transport effectively.

**Acknowledgments.** This research was supported by Basic Science Research Program through the National Research Foundation of Korea (NRF) funded by the Ministry of Education, Science and Technology (NRF20110016989) and by Priority Research Centers Program through the NRF (20110018396).

## References

1. Marrocchi, F. A.; Seri, M.; Kim, C.; Marks, T. J.; Facchetti, A.; Taticchi, A. *J. Am. Chem. Soc.* **2010**, *132*, 6108.
2. Park, S. K.; Jackson, T. N.; Anthony, J. E.; Mourey, D. A. *Appl. Phys. Lett.* **2007**, *91*, 063514.
3. Zhang, Y.; Petta, J. R.; Ambily, S.; Shen, Y.; Ralph, D. C.; Malliaras, G. G. *Adv. Mater.* **2003**, *15*, 1632.
4. Ha, J. S.; Kim, K. H.; Choi, D. H. *J. Am. Chem. Soc.* **2011**, *133*, 10364.
5. Zhang, L.; Tan, L.;Wang, Z.; Hu, W.; Zhu, D. *Chem. Mater.* **2009**, *21*, 1993.
6. (a) Li, H.; Valiyaveettil, S. *Tetrahedron Lett.* **2009**, *50*, 5311. (b) Wang, C.; Liu, Y.; Ji, Z.; Wang, E.; Li, R.; Jiang, H.; Tang, Q.; Li, H.; Hu, W. *Chem. Mater.* **2009**, *21*, 2840.
7. (a) Hoang, M. H.; Cho, M. J.; Kim, K. H.; Lee, T. W.; Jin, J. I.; Choi, D. H. *Chem. Lett.* **2010**, *39*, 396. (b) Pisula, W.; Menon, A.; Stepputat, M.; Lieberwirth, I.; Kolb, U.; Tracz, A.; Sirringhaus, H.; Pakula, T.; Müllen, K. *Adv. Mater.* **2005**, *17*, 684.
8. Ahmed, M. O.; Wang, C. M.; Keg, P.; Pisula, W.; Lam, Y. M.; Ong, B. S.; Ng, S. C.; Chen, Z. K.; Mhaisalkar, S. G. *J. Mater. Chem.* **2009**, *19*, 3449.
9. Hunziker, C.; Zhan, X.; Losio, P. A.; Figi, H.; Kwon, O. P.; Barlow, S.; Guenter, P.; Marder, S. R. *J. Mater. Chem.* **2007**, *17*, 4972.
10. Kim, K. H.; Chi, Z.; Cho, M. J.; Jin, J.-I.; Cho, M. Y.; Kim, S. J.; Joo, J.-S.; Choi, D. H. *Chem. Mater.* **2007**, *19*, 4925.
11. Hur, J. A.; Bae, S. Y.; Kim, K. H.; Lee, T. W.; Cho, M. J.; Choi, D. H. *Org. Letter.* **2011**, *13*, 1948.
12. Hodge, P.; Power, G. A.; Rabjohns, M. A. *Chem. Commun.* **1997**, 73.
13. Zhang, H. C.; Guo, E. Q.; Zhang, Y. L.; Ren, P. H.; Yang, W. J. *Chem. Mater.* **2009**, *21*, 5125.
14. Kim, K. H.; Bae, S. Y.; Kim, Y. S.; Hur, J. A.; Hoang, M. H.; Lee, T. W.; Cho, M. J.; Kim, Y.; Kim, M.; Jin, J.-I.; Kim, S.-J.; Lee, K.; Lee, S. J.; Choi, D. H. *Advanced Materials* **2011**, *23*, 3095.
15. Cho, M. Y.; Kim, S. J.; Han, Y. D.; Kim, K. H.; Choi, D. H.; Joo, J. *Advanced Functional Materials* **2008**, *18*, 2905.
16. Johnson, N. M.; Chiang, A. *Appl. Phys. Lett.* **1984**, *45*, 1102.